CELL WALL POROSITY IN NORWAY SPRUCE WOOD AS AFFECTED BY HIGH-TEMPERATURE DRYING

*Marc Borrega**†‡*
PhD Candidate

Petri P. Kärenlampi
Professor
Faculty of Science and Forestry
University of Eastern Finland
PO Box 111, 80101
Joensuu, Finland

(Received September 2010)

Abstract. In this study, pore size distribution in wood after high-temperature drying followed by rewetting was investigated by differential scanning calorimetry. Nonfreezing water content of wood was lower than previously indicated considering the effect of phase change on specific heat capacity of water. High-temperature drying appeared to close cavities of the largest size in earlywood, particularly with increasing drying temperature and time. Pore closure by irreversible hydrogen bonding dominated the eventual creation of cavities by degradation of wood structural components. Stress relaxation within wood elements, favored by slow high-temperature drying, decreased the extent of drying microcracks in earlywood, manifested in lower nonfreezing water content.

Keywords: Differential scanning calorimetry (DSC), drying, hornification, nonfreezing water, specific heat capacity, thermoporosimetry, wood.

INTRODUCTION

Wood cell walls have a heterogeneous disordered structure with chemical adsorption sites and pores of varying size and shape often appearing in a hydrated state. The structure in the cell wall appears to vary as a function of position within an annual ring, ie between earlywood and latewood (Watson and Dadswell 1962; Page et al 1972; Erickson and Arima 1974). It has also been shown that thermal transitions of cell wall water differ between earlywood and latewood (Tynjälä and Kärenlampi 2001; Kärenlampi et al 2005).

In heterogeneous hydrated systems, the amount of water with depressed melting temperature is detectable using differential scanning calorimetry (DSC) (Rennie and Clifford 1977; Homshaw 1981; Ishikiriyama et al 1995). The depressed melting temperature can be interpreted as either a consequence of some material constituents being partially solubilized or material being microporous in such a way that surface tension of pure water depresses melting temperature of water because of small pore radius. The latter interpretation enables porosity investigation in terms of thermoporosimetry (Maloney et al 1998; Maloney and Paulapuro 1999, 2001).

Some water in hydrated porous systems does not freeze. This can be explained in a variety of ways. One of the simplest explanations is that in a space close in size to that of a molecule, there is not much room for molecular motion. Thus, matter appears solid-like, regardless of temperature, and no thermal transition between solid and liquid is recognized (Berlin et al 1970). Molecular mobility may also be decreased because of adsorption sites such as ionic groups, ultimately forming a polymer gel (Berthold et al 1994, 1996). Alternatively, one might explain existence of nonfreezing water (NFW) in terms of

* Corresponding author: marc.borrega@aalto.fi
† SWST member
‡ Present address: Department of Forest Products Technology, School of Chemical Technology, Aalto University, PO Box 16300, 00076, Aalto, Finland.

slowness of diffusion at low temperature and in small capillaries (Pouchlý et al 1979; Kärenlampi et al 2005). On this basis, water in the saturated porous cell wall can be divided into free water, freezing bound water, and NFW (Nakamura et al 1981). Free water is located in large pores and cavities and has similar thermodynamic properties as pure bulk water.

In wood drying, and particularly in high-temperature drying, at least three mechanisms may affect wood porosity. First, elevated temperatures induce thermal degradation of wood components (Stamm 1956; Esteves et al 2007; Borrega and Kärenlampi 2010), which may result in cavities forming within the cell wall. Stone and Scallan (1967) and Maloney and Paulapuro (1999) reported that removal of hemicelluloses and lignin during pulping created new pores within the fiber cell wall. Second, as water exits pores during drying, pore walls start to collapse, eventually evolving into pore closure by irreversible hydrogen bonding (Weise et al 1996; Park et al 2006). This is often called hornification. Third, anisotropic drying shrinkage of cell wall layers induces internal drying stresses, which can be large enough to damage wood cell walls (Van den Akker 1962; Kifetew et al 1998; Thuvander et al 2001). Changes in wood porosity caused by drying may be reversible after rewetting for a prolonged time (Tynjälä and Kärenlampi 2001).

Drying damage is manifested as microcracks irregularly distributed within the wood cell wall (Wallström and Lindberg 1999, 2000). This microscopic damage appears to be more pronounced in earlywood than in latewood sections (Thuvander et al 2001; Borrega and Kärenlampi 2010). Furthermore, NFW content in earlywood significantly increases after drying (Kärenlampi et al 2005). The only mechanism we are aware of that possibly induces NFW content increment is microscopic drying damage.

Detection of a first-order transition in terms of calorimetry requires detection of latent heat related to that transition. This can be done by dividing total applied/released heat into latent heat and sensible heat for the temperature change. Sensible heat related to temperature change can be computed provided heat capacity of the specimen is known. Somewhat problematic is that specific heat capacity changes in phase transformations. Specific heat capacity of liquid water is more than two times that of ice. In recent literature dealing with application of calorimetry to wood and pulp fibers, latent heat has been determined by integrating across a baseline characterizing heat capacity of the specimen. Heat capacity, in turn, has been determined by linearly interpolating between temperatures well below and well above the range of melting temperatures (Maloney et al 1998; Maloney and Paulapuro 2001; Kärenlampi et al 2003a, 2003b, 2005). Linear interpolation of heat capacity across such a temperature range is, however, generally incorrect. The result depends on selection of temperatures between which the interpolation is done. We favor a stepwise method in which change in specific heat capacity is considered within any temperature step. Details of such a computation follow.

In this article, we first present experimental arrangements for high-temperature drying experiments and thermoporosimetry analyses. We then present a small development in determining wood cell wall properties through calorimetry. Next, we report results regarding pore size distribution in wood. Thermodynamic behavior of hydrated earlywood and latewood was considered separately. Finally, mechanisms affecting cell wall porosity during high-temperature drying are discussed.

METHODS AND MATERIALS

Drying Experiments

The wood was Norway spruce (*Picea abies*) felled in Joensuu, Finland. Wood specimens 50 × 20 × 90 mm (longitudinal, tangential, radial) were prepared. All specimens were free of visible flaws. Six groups containing 12-14 specimens each were formed, and each group was subjected to a particular drying treatment in which temperature and drying rate

were controlled independently. Drying treatments were conducted in a 20-L stainless steel pressure vessel equipped with a temperature gauge, a pressure gauge, and a valve for removing water vapor. Removed water vapor was condensed in a container placed on a weight scale, which allowed monitoring changes in wood moisture content.

Before any drying experiment, initial wood moisture content was approximated by oven-drying six additional specimens at 103°C for 24 h. Each group of specimens was then weighed and placed in the vessel. A measured amount of liquid water was added to improve heating efficiency of the system. Temperature in the vessel was raised to 128°C, and the pressure valve was opened. Because the valve is in the upper part of the vessel, air exited first (hot air greater than 125°C is lighter than hot steam). After air removal, rapid water vapor removal followed until wood had about 45% MC. Thereafter, the drying process was started at a predetermined temperature and drying rate. Drying rate was controlled by operating the pressure valve. Change in wood moisture content is given by

$$\frac{dM}{dt} = kM \qquad (1)$$

where M (g/g) is wood moisture content, t (s) is drying time, and k (s^{-1}) is drying rate constant.

After rearranging and integrating, Eq 1 is transformed into

$$\ln M = kt + C \qquad (2)$$

where C is integration constant. For $t = 0$, $C = \ln M_0$, where M_0 is moisture content at the beginning of the drying process, ie approximately 45%.

After substituting and rearranging, Eq 2 can be rewritten as

$$M_t = M_0 e^{kt} \qquad (3)$$

where M_t is moisture content of wood at any time of the drying process.

At the end of the drying process, all dried specimens were removed from the vessel and weighed. Specimens were subsequently placed in a climate-controlled room at 19°C and 65% RH to attain equilibrium moisture content. Drying process parameters are shown in Table 1.

In the case of rapid drying experiments, it was not possible to reach moisture contents below 7% without significantly decreasing drying rate. This is the reason why the final moisture content reached during drying was somewhat higher for those specimens that were rapidly dried compared with more slowly dried specimens (Table 1). Moisture gradients within the vessel during water vapor removal resulted in a higher variability in the final moisture content of rapidly dried specimens, shown by the greater 95% confidence intervals, compared with more slowly dried specimens.

Thermoporosimetry Analyses

After reaching equilibrium moisture content, one specimen from each drying treatment was selected for thermoporosimetry analysis. An additional specimen to be used as a reference was prepared from undried wood stored in a freezer

Table 1. Experimental parameters for drying processes.[a]

Temperature (°C)	Drying rate (-10^{-6} s^{-1})	Final moisture content (%)	Mass loss (%)	EMC[b] (%)
110	88.4	7.5 ± 2.3	0.2 ± 1.3	10.3 ± 0.6
120	105.0	7.4 ± 2.4	0.1 ± 2.3	10.3 ± 0.6
130	134.0	6.7 ± 3.0	0.5 ± 1.4	9.8 ± 0.6
110	6.8	5.1 ± 0.7	1.5 ± 1.5	8.7 ± 0.3
120	8.0	3.4 ± 0.4	2.2 ± 3.0	7.8 ± 0.2
130	6.9	5.5 ± 1.9	6.1 ± 1.2	7.9 ± 0.5

[a] Mean values with 95% confidence interval.
[b] Equilibrium moisture content (EMC) of dried specimens after being placed at 19°C and 65% RH.

for a few months. For any selected specimen, 60-μm-thick wood slices were produced from both earlywood and latewood with a sliding microtome. Earlywood and latewood samples, containing five and three microtomed slices, respectively, were formed. At least three earlywood and latewood samples were prepared from each specimen. All samples were immersed in deionized water and kept in a refrigerator for a minimum of 10 da.

For thermoporosimetry analyses, each sample was chopped with a sharp knife and fitted in a sealed 40-μL aluminum pan. A small hole was then pierced in the pan to keep a constant pressure throughout the experiment. The pan was weighed and placed in a Mettler Toledo (Columbus, OH) 823e differential scanning calorimeter. This device measures energy absorbed or released by a sample during temperature change. The energy absorbed when water in a frozen sample melts during a temperature increment is the sum of latent heat and sensible heat. Latent heat is then used to determine amount of water melted within the temperature step by means of the specific heat of melting. The experimental step program used for thermoporosimetry analyses is shown in Table 2. For every melting temperature, a representative pore size (assuming a cylindrical pore shape) can be computed by the Gibbs-Thomson equation:

$$D = \frac{-4 \cdot V_m \cdot \sigma_{ls}}{\overline{H}_m \cdot \ln \frac{T_m}{T_0}} \qquad (4)$$

where D is pore diameter (m), V_m is molar volume of ice, σ_{ls} is surface tension at the ice–water interface (20.4 mN/m; Ishikiriyama et al 1995), H_m is specific heat of melting (334 J/g), T0 is melting temperature of bulk water (273.15 K), and Tm is depressed melting temperature.

The pore diameter corresponding to each depressed melting temperature is shown in Table 3.

After the DSC experiment, each pan was weighed and subsequently oven-dried at 103°C for 24 h. NFW content was quantified by subtracting the amount of freezing water from the total amount of water in the sample. Dry mass of any sample was 4.9 ± 0.2 mg, and its basic density ranged from 210-349 kg/m^3 for earlywood and 509-826 kg/m^3 for latewood.

The thermodynamic properties of water were determined by conducting six DSC runs with only deionized water. The experimental program applied was the same as shown in Table 2. All energy absorbed by the water-only sample in the temperature interval –38 to –36°C and 4-5°C was considered to be a measure of its heat capacity. Average values for heat capacity of ice (Cp_i) and liquid water (Cp_w) were 1.85 and 4.34 J/(g·°C), respectively. Specific heat of melting was 338.3 J/g.

Table 2. Experimental step program for thermoporosimetry analyses in differential scanning calorimetry instrument.

Step, n	Initial temperature (°C)	Heating ramp (°C/min)	Final temperature (°C)	Holding time at final temperature (min)
1	25	−10	20	6
2	20	−10	4	6
3	4	−5	−38	6
4	−38	1	−30	6
5	−30	1	−10	6
6	−10	1	−3	6
7	−3	1	−1	6
8	−1	1	−0.5	6
9	−0.5	1	−0.2	9
10	−0.2	1	−0.1	12
11	−0.1	−5	−38	6
12	−38	1	−36	6
13	−36	5	4	9
14	4	1	5	9
15	5	10	25	—

Table 3. Pore diameter corresponding to depressed melting temperature, computed with Gibbs-Thomson equation (Eq 4).

Melting temperature (°C)	Pore diameter (nm)
−38	1.8
−30	2.3
−10	7.2
−3	24.2
−1	72.7
−0.5	145.6
−0.2	364.1
−0.1	728.4

Data Analysis

Because of the small hole pierced in the aluminum pan, some water evaporated during the DSC experiment. Total amount of water evaporated was determined by weighing the pan immediately before and after the test. In addition, the amount of water evaporated was computed through signal values (mW) given by the DSC instrument, duration of any temperature step, and specific heat of vaporization (2260 J/g). Good agreement was found between measured and computed values for evaporated water (Fig 1). Therefore, using the signal values given by the DSC instrument, the actual amount of water within the pan at any instant of the experiment could be accurately determined.

Melting enthalpy during any temperature step was computed by subtracting the amount of heat used in increasing temperature, ie heat capacity, from the total amount of energy absorbed by the sample. Heat capacity of any sample was determined, as in the case of water-only experiments, by measuring energy absorbed in the temperature range –38 to –36°C and 4-5°C. Heat capacity of the sample below 0°C, however, cannot be regarded as constant because it depends on the amount of water melting in each temperature interval (heat capacity of liquid water is higher than heat capacity of ice). Furthermore, heat capacity of ice is temperature-dependent, increasing about 10% from –38 to –10°C (Giauque and Stout 1936). Thus, heat capacity of any sample at a temperature step n below 0°C (Table 2) was computed as

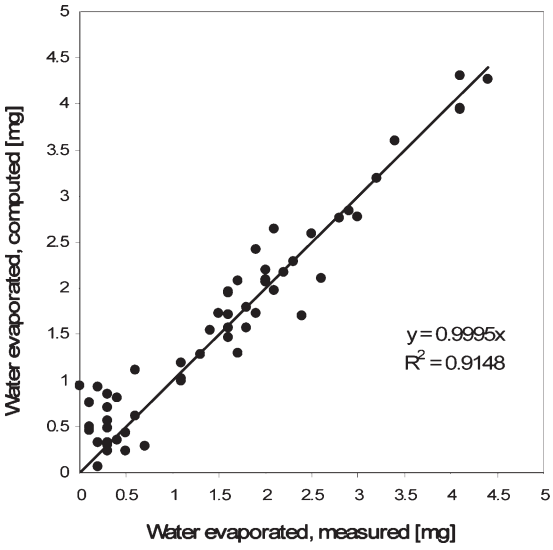

Figure 1. Water evaporated from wood sample during differential scanning calorimetry (DSC) experiments. Values computed from DSC readings are plotted vs values measured by gravimetry.

for $n = 4$,

$$Cp_n = (Cp_0 + (W_n \cdot Cp_i) \cdot (1.05 - 1)) + Wm_n(Cp_w - 1.05\,Cp_i) \quad (5)$$

for $n = 5$,

$$Cp_n = \left(Cp_{n-1} + (W_n \cdot Cp_i) \cdot (1.05^2 - 1.05)\right) + Wm_n(Cp_w - 1.05^2\,Cp_i) \quad (6)$$

for $n = 6, \ldots 10$,

$$Cp_n = Cp_{n-1} + Wm_n(Cp_w - 1.05^2 Cp_i) \quad (7)$$

where Cp_n, W_n, and Wm_n are heat capacity of the sample, mass of water in the sample, and mass of melted water in temperature step n, respectively; Cp_0 is heat capacity of the sample between –38 and –36°C; and Cp_w and Cp_i are measured heat capacity of liquid water and ice, respectively.

Eq 7 may be used to compute heat capacity of the sample between –0.1 and 4°C, which should equal heat capacity measured between 4 and 5°C. The consistency of this kind of treatment is shown in Fig 2, where heat capacity of liquid water computed with Eqs 5-7 is plotted vs heat capacity of water measured from 4-5°C.

RESULTS AND DISCUSSION

Pore size distribution in earlywood and latewood after high-temperature drying followed by rewetting was investigated by DSC. Cumulative pore water, expressed in relation to dry wood mass, is plotted vs pore size in Fig 3. Accordingly, NFW content appeared to be predominantly between 20 and 30% of dry wood mass. Recent studies indicate that NFW content

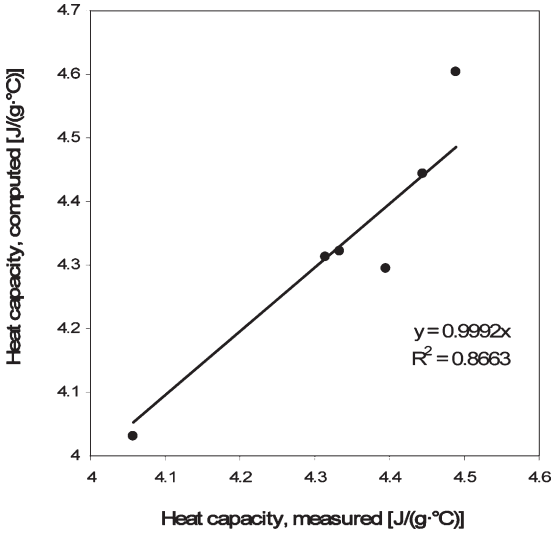

Figure 2. Heat capacity of liquid water (Cpw) computed with Eqs 5-7, plotted vs heat capacity of liquid water measured in temperature range 4-5°C.

of dried wood specimens is within 30-40% (Maloney and Paulapuro 1999; Tynjälä and Kärenlampi 2001; Kärenlampi et al 2005). An obvious explanation for this difference is that these studies have not succeeded in determining specific heat capacity correctly. Heat capacity changes along with a thawing process. Literature values indicate overestimated heat capacity, consequently underestimated amount of melting water, and finally overestimated NFW content.

A very small difference was found in the amount of NFW between earlywood and latewood, the average values being 0.23 g/g and 0.25 g/g, respectively (Fig 3). Similar NFW content in dried earlywood and latewood has also been reported by Kärenlampi et al (2005). They found that drying increased the amount of NFW in earlywood. This phenomenon was not detected in this study (Fig 3a), possibly because reference specimens were stored in a freezer for a few months, which might have induced some freeze-drying.

Up to 24-nm pore size, both earlywood and latewood appear to have similar pore size distribution, indicated by the amount of pore water (Fig 3). However, earlywood contains more

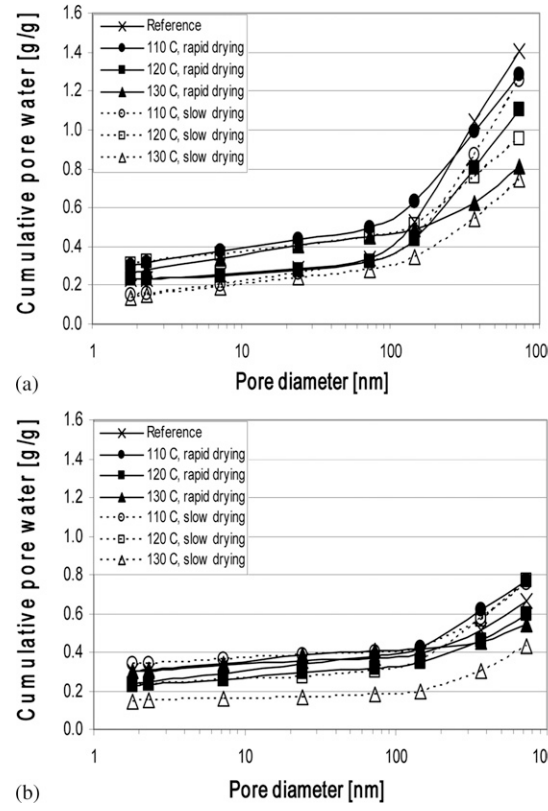

Figure 3. Cumulative pore water per dry wood mass as function of pore size in (a) earlywood and (b) latewood.

pores of larger size with almost twice as much pore water as latewood in pores of 300-800 nm. The greater porosity of earlywood may be related to higher density of pits between fibers (Sirviö and Kärenlampi 1998). Nonetheless, it is remarkable that in a few earlywood samples, the total amount of bound water well exceeds the dry mass of wood (Fig 3a). Such a high amount of pore water may be associated with artifacts created when microtoming. Porosity may also depend on rewetting time.

Eventual effects of microtoming and rewetting time were investigated by preparing undried earlywood samples with 60- and 200-µm-thick microtomed slices and keeping them immersed in deionized water for 48 h before the DSC experiment. Results are shown in Fig 4, and data from reference earlywood samples in Fig 3a are included for comparison. Up to

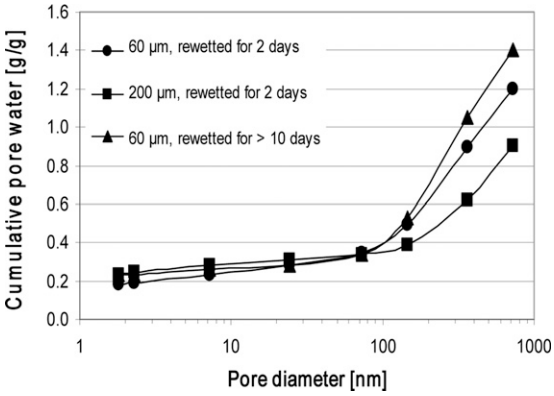

Figure 4. Effect of thickness and rewetting time of microtomed earlywood samples on pore size distribution in cell wall.

73-nm pore size, pore water content in all earlywood samples appeared to be nearly identical. Increasing rewetting time appeared to open up pores larger than 145 nm.

Earlywood samples of 200-µm thickness clearly showed the lowest bound water content (Fig 4). Preparing wood slices with a sliding microtome appeared to create new cavities in the cell wall because of mechanical damage. The thinner the microtomed wood slice, the more damage it experienced. This effect was clearly most pronounced in the thin-walled earlywood fibers (Fig 3).

In this study, a pierced pan was used in DSC experiments instead of a sealed pan, which was used previously (Maloney and Paulapuro 1999; Tynjälä and Kärenlampi 2001; Park et al 2006). This obviously affected the depressed melting temperature of water as a function of pore size. With a pierced pan, pressure is atmospheric, regardless of temperature. With a sealed pan, however, pressure changes as a function of temperature. The wood sample is probably placed in the pan at room temperature, and lower temperatures within the pan correspond to lower pressure. Then, melting temperature of water in a sealed pan is slightly higher than that at atmospheric pressure. Consequently, at any depressed melting temperature, corresponding pore size as given by the Gibbs-Thomson equation (Eq 4) becomes underestimated when using a sealed pan. The total amount of bound water determined in a sealed pan might be somewhat lower than that determined in a pierced pan, because of some additional pore water eventually melting between –0.1°C and melting temperature of free water.

Regarding the effect of drying conditions on pore size distribution, it is believed that at least three mechanisms may alter pore structure in wood. First, thermal degradation of wood components after exposure to elevated temperatures may create new cavities in the cell wall (Stamm 1956; Esteves et al 2007; Borrega and Kärenlampi 2010). Second, irreversible hydrogen bonding among carbohydrate elements, ie hornification, promotes pore closure as water exits the pore (Weise et al 1996; Park et al 2006). Third, microscopic damage caused by anisotropic shrinkage of cell wall layers results in microcracks within the porous cell wall, particularly in earlywood (Wallström and Lindberg 1999, 2000; Thuvander et al 2001; Borrega and Kärenlampi 2010).

According to Fig 3a, earlywood sections in all dried specimens contained less bound water than native earlywood. Drying appears to close cavities of the largest size (greater than 145 nm), whereas no clear effect on the smaller pores can be observed. Furthermore, the amount of bound water in dried earlywood appears to decrease with increasing drying temperature and time. Apparent closure of cavities implies formation of irreversible hydrogen bonds within the cell wall during high-temperature drying, in particular with extended drying times, as previously proposed by Borrega and Kärenlampi (2010).

Earlywood and latewood sections from specimens slowly dried at 130°C had the lowest amount of bound water, regardless of pore size (Fig 3) and despite the fact that these specimens had the greatest mass loss (Table 1). Therefore, pore closure promoted by irreversible hydrogen bonding appeared to dominate the creation of new cavities by degradation of wood components. On a macroscopic level, closure of pores

by irreversible hydrogen bonding within the wood structure and mass loss caused by degradation of hygroscopic hemicelluloses resulted in wood specimens with lower equilibrium moisture content (Table 1).

Anisotropic drying shrinkage of cell wall elements results in microcracks within the porous structure of dried wood (Wallström and Lindberg 1999, 2000). Incompatibility of drying shrinkage is pronounced when microfibril angle varies between and within cell wall layers (Van den Akker 1962). In wood fibers, the S1 and S3 layers have large and widely varying microfibril angles (Paakkari and Serimaa 1984). Thus, microscopic drying damage is likely to be more significant in those fibers with a smaller proportion of S2 layer, ie in earlywood fibers. In fact, NFW content of earlywood has been reported to increase considerably after drying (Kärenlampi et al 2005), obviously caused by microscopic drying damage.

Internal drying stresses within the wood cell wall and the consequent formation of microcracks may be decreased by conducting slow drying processes at high temperatures. This is because stress relaxation within wood elements, caused by molecular reorganization, is favored by an increase in available time, moisture content, and temperature (Williams et al 1955; Kelley et al 1987).

A decreased amount of microcracks, caused by stress relaxation, may have been partly responsible for the lower amount of bound water in dried earlywood along with increasing drying temperature and time (Fig 3a). In particular, slow drying processes appeared to result in lower NFW content in earlywood (Fig 3a). In latewood sections, however, microscopic cell wall damage was less pronounced, and thus, effects of stress relaxation on cell wall porosity cannot be clearly identified (Fig 3b). Further investigation of pore size distribution of dried earlywood and latewood is needed to elucidate the effects of hornification and microscopic drying damage on the cell wall structure of dried wood.

CONCLUSIONS

Wood cell wall porosity, after high-temperature drying followed by rewetting, was investigated by DSC. NFW content in earlywood and latewood, both in never-dried and dried wood samples, was predominantly between 20 and 30% of the dry wood mass. Both earlywood and latewood contain a similar amount of pores of the smallest size. However, earlywood has a greater density of pores larger than 24 nm with as much as twice the amount of bound water compared with latewood. Total amount of bound water in earlywood cell walls appeared to be remarkably high, probably related to creation of cavities (artifacts) during sample preparation and to prolonged rewetting times of wood samples.

Drying appears to close cavities of the largest size in earlywood sections. Amount of bound water in dried earlywood decreased with increasing drying temperature and time. This was believed to be caused by pore closure induced by irreversible hydrogen bonding during high-temperature drying, in particular with extended drying time. Pore closure appeared to prevail over creation of cavities by degradation of wood structural components. Stress relaxation within wood elements, favored by slow high-temperature drying, decreased the extent of drying microcracks within the cell wall, which was manifested in lesser NFW content in earlywood.

ACKNOWLEDGMENTS

We thank Dr. Leila Alvila of the Department of Chemistry, University of Eastern Finland, for the advice and support with the DSC experiments. Funding from Niemi-säätiö granted to Marc Borrega is gratefully acknowledged.

REFERENCES

Berlin E, Kliman PG, Pallansch MJ (1970) Changes in state of water in proteinaceous systems. J Colloid Interface Sci 34:488-494.

Berthold J, Desbrières J, Rinaudo M, Salmén L (1994) Types of adsorbed water in relation to the ionic groups and their counter-ions for some cellulose derivatives. Polymer (Guildf) 35:5729-5736.

Berthold J, Rinaudo M, Salmén L (1996) Association of water to polar groups; Estimations by an adsorption model for ligno-cellulosic materials. Colloid Surface A 112:117-129.

Borrega M, Kärenlampi PP (2010) Three mechanisms affecting the mechanical properties of spruce wood dried at high temperatures. J Wood Sci 56:87-94.

Erickson HD, Arima T (1974) Douglas-fir wood quality studies. Part II: Effects of age and stimulated growth on fibril angle and chemical constituents. Wood Sci Technol 8:255-265.

Esteves B, Marques AV, Domingos I, Pereira H (2007) Influence of steam heating on the properties of pine (*Pinus pinaster*) and eucalypt (*Eucalyptus globulus*) wood. Wood Sci Technol 41:193-207.

Giauque WF, Stout JW (1936) The entropy of water and the third law of thermodynamics. The heat capacity of ice from 15 to 273 K. J Am Chem Soc 58:1144-1150.

Homshaw LG (1981) Calorimetric determination of porosity and pore size distribution (PSD): Effect of heat on porosity, pore form, and PSD in water-saturated polyacrylonitrile fibers. J Colloid Interface Sci 84:127-140.

Ishikiriyama K, Todoki M, Motomura K (1995) Pore size distribution (PSD) measurements of silica gels by means of differential scanning calorimetry. I. Optimization for determination of PSD. J Colloid Interface Sci 171:92-102.

Kärenlampi PP, Tynjälä P, Ström P (2003a) Molecular fatigue in steamed wood. Int J Fatigue 25:489-497.

Kärenlampi PP, Tynjälä P, Ström P (2003b) Molecular reorganization in wood. Mech Mater 35:1149-1159.

Kärenlampi PP, Tynjälä P, Ström P (2005) Phase transformations of wood cell wall water. J Wood Sci 51:118-123.

Kelley SS, Rials TG, Glasser WG (1987) Relaxation behaviour of the amorphous components of wood. J Mater Sci 22:617-624.

Kifetew G, Thuvander F, Berglund L, Lindberg H (1998) The effect of drying on wood fracture surfaces from specimens loaded in wet condition. Wood Sci Technol 32:83-94.

Maloney TC, Paulapuro H (1999) The formation of pores in the cell wall. J Pulp Paper Sci 25:430-436.

Maloney TC, Paulapuro H (2001) Thermoporosimetry of pulp fibres. Pages 897-926 *in* 12th Fundamental Research Symposium, 2001, Oxford, UK.

Maloney TC, Paulapuro H, Stenius P (1998) Hydration and swelling of pulp fibers measured with differential scanning calorimetry. Nord Pulp Pap Res J 13:31-36.

Nakamura K, Hatakeyama T, Hatakeyama H (1981) Studies on bound water of cellulose by differential scanning calorimetry. Textile Res J 51:607-613.

Paakkari T, Serimaa R (1984) A study of the structure of wood cells by X-ray diffraction. Wood Sci Technol 18:79-85.

Page DH, El-Hosseiny F, Winkler K, Bain R (1972) The mechanical properties of single wood-pulp fibres. Part 1: A new approach. Pulp Pap-Canada 73:72-77.

Park S, Venditti RA, Jameel H, Pawlak JJ (2006) Changes in pore size distribution during the drying of cellulose fibers as measured by differential scanning calorimetry. Carbohydr Polym 66:97-103.

Pouchlý J, Biros J, Benes S (1979) Heat capacities of water swollen hydrophilic polymers above and below 0°C. Makromol Chem 180:745-760.

Rennie GK, Clifford J (1977) Melting of ice in porous solids. Journal of the Chemical Society, Faraday Transactions 1: Physical Chemistry in Condensed Phases 73:680-689.

Sirviö J, Kärenlampi P (1998) Pits as natural irregularities in softwood fibers. Wood Fiber Sci 30:27-39.

Stamm AJ (1956) Thermal degradation of wood and cellulose. Ind Eng Chem 48:413-417.

Stone JE, Scallan AM (1967) The effect of component removal upon the porous structure of the cell wall of wood. II. Swelling in water and the fiber saturation point. Tappi 50:496-501.

Thuvander F, Wallström L, Berglund LA, Lindberg KAH (2001) Effects of an impregnation procedure for prevention of wood cell wall damage due to drying. Wood Sci Technol 34:473-480.

Tynjälä P, Kärenlampi PP (2001) Spruce cell wall porosity. Variation within annual ring and drying response. Pages 39-45 *in* First International Conference of the European Society for Wood Mechanics, 2001, Lausanne, Switzerland.

Van den Akker JA (1962) Some theoretical considerations on the mechanical properties of fibrous structures. Pages 201-241 *in* F Bolam, ed. Formation and structure of paper. Vol. 1. Transactions of the symposium held at Oxford, September 1961, Technical Section of the British Paper and Board's Makers Association, London, UK.

Wallström L, Lindberg KAH (1999) Measurement of cell wall penetration in wood of water-based chemicals using SEM/EDS and STEM/EDS technique. Wood Sci Technol 33:111-122.

Wallström L, Lindberg KAH (2000) Distribution of added chemicals in the cell walls of high temperature dried and green wood of Swedish pine, Pinus sylvestris. Wood Sci Technol 34:327-336.

Watson AJ, Dadswell HE (1962) Influence of fibre morphology on paper properties. II. Early wood and late wood. Appita 15:116-128.

Weise U, Maloney T, Paulapuro H (1996) Quantification of water in different states of interaction with wood pulp fibres. Cellulose 3:189-202.

Williams ML, Landel RF, Ferry JD (1955) Temperature dependence of relaxation mechanisms in amorphous polymers and other glassforming liquids. J Appl Physics 77:3701-3706.